# Micelles templated NiO hollow nanospheres as anode materials in lithium ion batteries

**Manickam Sasidharan\*[a,b], Nanda Gunawardhana,[a] Senthil Chenrayan[b] and Masaki Yoshio[a\*]**

[a]*Advanced Research Center, Saga University, 1341 Yogamachi, Saga, 840-0047, Japan.*

[b]*SRM Research Institute, SRM University, Kattankulathur, Chennai 603 203, India.*

Nano-sized nickel oxide (NiO) hollow spheres of size $28 \pm 2$ nm have been synthesized by soft-template self-assembly process. ABC triblock copolymeric micelles of poly(styrene-*b*-acrylic acid-*b*-ethylene oxide) (PS-PAA-PEO) with *core-shell-corona* architecture serve as an efficient colloidal-template for fabrication of NiO hollow nanospheres. In the above polymeric template, the PS block (*core*) acts as template of hollow void space, the PAA block (*shell*) with negative charges serves as reaction site for metal ion interactions, and the *corona* domain stabilizes organic/inorganic composite particles. The PS-PAA-PEO template micelles as well as the NiO hollow nanospheres were thoroughly characterized by dynamic light scattering (DLS), transmission electron microscope (TEM), X-ray diffraction (XRD), thermal analysis (TG/DTA), FTIR spectroscopy, and nitrogen adsorption/desorption analyses. The XRD and TEM techniques confirmed the hollow spherical morphology and phase purity of nickel oxide nanoparticles. The NiO hollow nanospheres were further investigated as anode materials for lithium ion rechargeable batteries for the first time. The nanostructured electrode delivers high capacity of 393 mAh g$^{-1}$ after 50 cycles of charge/discharges at a rate of 0.3 C. More importantly, the hollow spherical electrode maintains the structural integrity and excellent cycling stability even after subjecting to high rate of 10 C (high current density). The high electrochemical

performance is attributed to hollow void space coupled with nanosized NiO shell domain that facilitates fast lithium diffusion kinetics.

## Introduction

Nanostructures of traditional electrode materials, because of their novel properties associated with decreased size, and unique shape have been widely studied and demonstrated to exhibit superior characteristics to the bulk counterparts. The topology and morphology control of nanoparticles is very crucial in order to promote the desired industrial applications. Hollow spherical structures as an unusual morphological class of materials have meanwhile evoked manifold interest. The hollow colloidal particles are exceptionally promising materials in diverse fields of technology including catalysis, drug delivery, photonics, biotechnology, and electrochemical cell due to high surface area, low specific weight, and enhanced mechanical strength.[1-6] The recent upsurge in reports of novel template-free route for the preparation of hollow particles [7-10] underscores their importance and highlights the range of approaches that can be used for their synthesis. Notwithstanding these advances, templating against colloidal particles remains arguably the most effective, and certainly the most attractive method for the preparation of hollow particles with a narrow size distribution and well-defined shape.[11-15] Two general approaches widely employed to produce hollow structures are by templating against hard particles (hard-templates) and soft-template synthesis. In the case of hard-template strategy, monodispersed polymer latex and silica spheres are commonly used as colloidal templates because they are readily available in a wide range of sizes.[1,11-15] For instance, $TiO_2$ and $SnO_2$ hollow particles were reported by using three-dimensional latex arrays or their replicas as hard templates.[16-18] A common difficulty in hard-template based syntheses arises from the well-known

challenge of creating uniform coatings of desired materials (or their precursors) on the corresponding templates. In many cases incompatibility between the substrate and coating material requires prior surface modification/functionalization before the coating step can be performed.

Recently, soft-template directed approaches, such as direct replication of preformed structures and organized reaction environments have been used extensively to synthesis hollow spherical particles. For example, silica hollow particles were extensively studied through layer-by-layer self-assembly, the $EO_{76}$–$PO_{29}$–$EO_{76}$/butanol/ethanol/$H_2O$ quaternary system, and O/W micro-emulsion techniques.[1,19-22] Especially, polymer nanoparticles such as latexes and polymeric micelles were widely used because it is easy to control the size, morphology, and surface functionality of these soft-templates. It is important to mention that, the latex particles generally lead to hollow particles with relatively large diameter ranging from sub-micrometers to micrometers; whereas polymeric micelles are used for synthesis of hollow particles with diameters lower than one hundred nanometers. However, templates of polymeric micelles have been scarcely studied compared to latex particles based templates for preparation of metal oxide hollow nanospheres. The advantage of polymeric micelles over latex particles is that they can be easily formed with different chemical compositions as well as block lengths. Recently, we demonstrated a novel strategy in which ABC triblock copolymer micelles with a *core-shell-corona* structure are used as a template.[23,24] In our system, the *core* acts as template for creation of hollow void space, the *shell* serves as reaction sites for inorganic precursors and the *corona* stabilizes composite particles. Using this approach, we have reported $TiO_2$, $La_2O_3$, $V_2O_5$, and $MoO_3$ [25-28] hollow nanospheres with compositionally different ABC triblock copolymers. Herein, we report on the fabrication of nickel oxide (NiO) hollow nanospheres using micelles of

poly(styrene-*b*-acrylic acid-*b*-ethylene oxide) (PS-PAA-PEO) as a soft template (scheme 1) and also investigated these hollow nanospheres as negative electrode (anode) materials for lithium-ion rechargeable batteries.

Owing to their superior properties, NiO has been under extensive investigation as an important functional inorganic material for fuel cells,[29] solar cells,[30] Li-ion batteries (LIBs) and supercapacitors.[31-33] Nanomaterials can alter electrochemical conditions by reducing particle size vis-à-vis Li-ion diffusion length. This point is clearly illustrated in the transition metal oxide system by considering the applicability of these nanomaterials to Li-ion batteries.[34,35] Nano/microscaled electrode materials with small crystallite size possess high surface area, large surface-to-volume ratio, and favorable structural stability. These characteristics are beneficial to the electrochemical properties because they would lead to fast Li-ion/electron transfer, sufficient contact between active materials and electrolyte, and enhanced flexibility. These attributes generally lead to improved electrode performances such as higher overall capacity, better high-rate capability, and longer cycling life Li-ion batteries. In view of these developments, the NiO hollow nanosphere was investigated as negative electrode materials in Li-ion rechargeable batteries. The hollow nanospheres based electrode exhibits a high discharge capacity of 393 mAhg$^{-1}$, high rate capability, and columbic efficiency.

**Experimental section**

**Preparation of PS−PAA−PEO micelles and hollow nanospheres**

Nickel nitrate $Ni(NO_3)_2.5H_2O$ and $NH_4OH$ were obtained from Wako pure chemicals. $PEO_{47}$−*b*−$PAA_{90}$−*b*−$PS_{80}$ was synthesized *via* RAFT-controlled radical polymerization as shown in Scheme S1 in supporting information (ESI). The required amount of triblock copolymer PS–PAA–PEO

was dissolved in distilled water by stirring at room temperature for several days to obtain 0.5 gL$^-$$^1$ micelle solutions. Then the pH was adjusted to 9.5 using a dilute $NH_4OH$ solution. The hollow nanosphere synthesis was carried out ($Ni^{2+}$/PAA = 8) at room temperature excluding the hollowing step which was performed at 500 °C (Scheme 1). A desired amount of $Ni(NO_3)_2.5H_2O$ was added to polymeric micelle solution (10 mL) and stirred for a while and the clear solution slowly turns to a pale green gelatinous precipitate. The composite particles were aged at room temperature for two days without agitation. The solid product was separated by centrifugation, washed thoroughly with distilled water and ethanol followed by drying at 60 °C. Finally, the core/shell particles were heated at 500 °C for simultaneous removal of the remaining polymeric templates as well as to crystallize the amorphous hollow particles.

**Lithium insertion studies over hollow NiO nanospheres**

For lithium insertion studies, the NiO hollow nanosphere (5.0 mg) was mixed mechanically with Teflonized acetylene black (TAB-2, 2.0 mg) and then the mixture was pressed on a stainless steel mesh as the current collector under a pressure of 500 kg/cm$^2$ and dried at 160 °C for 4 hours under vacuum. The electrochemical characterizations were carried out using CR-2032 coin type cells with lithium as an anode. The electrolyte used was 1M $LiPF_6$-EC:DMC (1:2 by volume, Ube Chemicals Co. Ltd.). The coin cell assembling was performed in a glove box filled with argon (dew point, lower than −80 $^\circ$C). The galvanostatic charge–discharge tests of the coin cell were performed at the constant current density of 0.5 mAcm$^{-2}$.

**Characterization**

Powder X-ray diffraction (XRD) patterns were measured on a Rigaku RINT-2200 diffractometer with CuKα radiation (40 kV, 30 mA) from 10° to 70° 2θ in 0.02 steps at a scan speed of 2° min$^-$

[1]. DLS measurements were carried out with an Otsuka ELS-8000 electrophoretic light scattering spectrophotometer at a fixed 90 degree scattering angle. The hydrodynamic diameter ($D_h$) was calculated from $D$ using the Stokes-Einstein equation: $D_h = k_B T / 3\pi\eta D$, where $k_B$ is the Boltzmann constant, $T$ the absolute temperature, and $\eta$ the solvent viscosity. The TEM pictures were recorded on JEOL JEM-1210 Electron Microscope operating at 80 kV and JEOL 2010 (200 kV). In the case of micelle solutions, the TEM samples were prepared by casting a drop of micelle solution on a copper grid followed by staining with 1 wt% phosphotungstic acid; whereas for hollow NiO particles, a drop of water suspension was coated on a copper grid. The samples were finally dried at room temperature. Fourier transform infrared (FTIR) spectra were recorded on a Jasco FT/IR 7300 spectrometer using KBr pellet technique. Thermogravimetric and differential thermograms (TG-DTA) were obtained with MAC Science TG-DTA 2100 under air. BET surface area was measured by $N_2$ adsorption/desorption analysis at 77 K on a BELSORB 28SA analyzer after evacuation at 300 °C for 4 h.

**Results and discussion**

The triblock copolymer $PS_{80}$–$PAA_{90}$–$PEO_{47}$ was synthesized by controlled radical polymerization and the details are provided in the supporting information Scheme S1 (Fig. S1-S3, ESI).[36] Prior to synthesis of hollow NiO nanospheres, the PS–PAA–PEO micelles (Scheme 1, step 1) were characterized by DLS and TEM to confirm the spherical morphology. The hydrodynamic diameter $D_h$ and the ζ-potential (−52 mV) of the template micelles (pH 9.5) were obtained from dynamic light scattering (DLS) and electrophoretic light scattering (ELS) experiments. The negative value of ζ-potential confirms that the surface of micelle particles is composed of −COO⁻ anions. The typical average $D_h$ of PS–PAA–PEO obtained by DLS at pH

9.5 was found to be 65 nm. The morphology of template micelles was confirmed by TEM observation after staining the micelles with phosphotungstic acid and nearly monodispersed spherical micelles with average diameter *ca*. 48 ± 1 nm were estimated (Fig.1). The difference in the micelle particles' size between DLS and TEM is due to the fact that the latter accounts for only the *core–shell* part and excludes *corona* part of the micelle. The white contrast in the TEM image indicates the hydrophobic PS-core domain; similar to PS–PVP–PEO micelles,[37] the PS–PAA–PEO micelles under present study also contain a glassy hydrophobic PS core, an ionizable hydrophilic PAA shell, and hydrophobic PEO corona. In alkaline medium (> 7), the PAA block containing −COOH ($PK_a$ 4.6) exists in the deprotonated form (−COO⁻) and the PAA shell domain expands due to repulsive forces among the negatively charged PAA units. On gradual addition of $Ni^{2+}$ to the micelle solution (Scheme 1, step 2), the ζ-potential ( −52 mV) slowly changes to zero indicating the effective interaction of −COO⁻ anions with $Ni^{2+}$ cations (Fig.2). In Fig.2, the degree of neutralization is expressed as the ratio of amount of added $Ni^{2+}$ ion to the amount of acrylic acid in the PAA block. The schematic representation of formation of NiO hollow nanospheres is shown in the Scheme 1. Evidence for formation of composite particles through electrostatic interaction of $Ni^{2+}$ with −COO⁻ anions is also obtained from FTIR spectra (Fig. S4, curve A) of the composites that clearly shows strong band at 1602 cm⁻¹ which is red shifted from the carboxyl group stretching vibration that usually appears at 1735 cm⁻¹. Furthermore, bands at 1370–1620 cm⁻¹ is attributed to −C=C− bond stretching vibration of phenyl groups of the polymer backbone. After calcinations, these bands were completely disappeared indicating complete removal of the polymeric templates (Fig. S4; curve B). It is worthwhile to mention that most of polymeric templates were removed during the repeated washing with water and ethanol because the PS–PAA–PEO is a water soluble polymer. The

FTIR results are further corroborated with thermal analyses (TG/DTA) that confirmed the complete decomposition of polymers below 500 °C (Fig.S5).

The crystallinity and phase purity of the composite particles $Ni(OH)_2$ and NiO hollow nanospheres were examined by powder XRD as shown in Fig.3. The composite particles exclusively comprised of $\alpha$-$Ni(OH)_2$ phase (JCPDS-ICDD card 38-0715). After calcinations at 500 °C, the composite particles ($Ni(OH)_2$) undergo dehydration to form NiO and the XRD pattern (Fig.3, B) corresponds well with standard crystallographic data of NiO (JCPDS-ICDD card 01-1237, Bunsenite mineral).[38] The structure is a cubic unit cell with three main diffraction peaks at 37.4, 43.5, and 62.5 corresponding to (111), (200), and (220) reflections, respectively. The morphology and microstructures evolution of NiO nanostructures at different synthesis temperature have been examined by transmission electron microscopy (TEM) as shown in Fig. 4. Almost all the NiO hollow nanoparticles show a uniform spherical shape with a smooth shell wall (Fig. 4A) for samples synthesized at room temperature sol-gel reaction. The average particles size estimated from TEM observations was found to be 28 ± 2 nm; whereas the void space diameter and shell thickness were 17 ±1 and 11 ± 1 nm, respectively. Although, the template micelle size was about 48 ± 1 nm, the size of the NiO hollow nanosphere is only 28 ± nm and this result indicates that the NiO hollow nanospheres shrunk during the calcinations.[39,40] Furthermore, hollow particles tend to aggregate easily due to very high surface energy as is seen from TEM image (particles with dark contrast). The high resolution transmission electron microscope (HRTEM) allows the lattice fringes of NiO nanocrystals and confirms the crystalline nature of the shell domain (Fig. 4B). The lattice spacing of about 0.21 nm corresponds to the d spacing between adjacent (200) planes of NiO crystals.[41]

Furthermore, the size and shape of block copolymer self-assembled structures can be sensitive to external stimuli, such as concentration, pH, solvent, and temperature.[42] Temperature- and pH-sensitive *core–shell–corona* micelles having a PS *core*, a polyvinylpyridine (P2VP) *shell*, and a PEO corona have also been reported.[43] It is important to note that, the sol-gel reaction temperature and aging time play an important role in controlling a particular morphology. Thus the aging of reaction mixture or composite particles at 90 °C leads to transformation of initially formed spherical to rod-like morphology (Fig.4C). Therefore, for formation of hollow spherical morphology, the synthesis was performed under room temperature sol-gel reaction. The hollow particles appear to aggregate to certain extent as seen from TEM image (Fig.4A) mainly due to very high surface energy of nanoparticles coupled with absence of stabilizing agents. However, at high temperatures, the NiO hollow nanospheres tend to form nanorods (closed- and open-ends) through aggregation of spherical nanoparticles and TEM image (Fig.4C) clearly shows the product obtained after 48 h of sol-gel reaction at 90 °C. At extended reaction times, all the nanospheres were transformed in to bundles of nanorods (Fig. 4D). Thus at high temperature, the *core*-forming blocks are expected to be stretched, and as a result, the energy of the *core–shell* interface is modified to favor rod-like morphology.[44] As our objective is to synthesize hollow nanospheres, we have not paid much attention to formation of isotrophic structure like nanotubes and will be dealt separately. Nitrogen adsorption/desorption isotherms of NiO hollow spherical particles resemble that of disordered mesoporous materials (Fig. S6). The pore-size distribution curves obtained from the adsorption branches of the isotherms on the basis of nonlinear density functional theory (NLDFT) model show the existence of disordered mesopores of size about 2.5-5 nm in the shell domain of hollow particles (Fig.S6, inset). The hollow particles also exhibit high surface area (91 m$^2$g$^{-1}$) and total pore volume (0.84

$cm^3g^{-1}$). Thus characterized NiO hollow nanospheres were used as a negative electrode material for lithium-ion batteries.

Cyclic voltammetry (CV) measurements were performed to examine the electrochemical properties of the NiO hollow nanospheres. Fig.5 presents the CV curves of NiO hollow nanospheres constructed electrode in the first and second cycle (first two complete cycles) performed at a sweep rate of 3 mV/min. from 0.005–3.0 V (vs. $Li^+$/Li). During the first cycle, NiO hollow nanosphere electrode shows a strong broad irreversible reduction peak with a maximum at 0.27 V (which extends up to 0.83 V) indicative of reduction of NiO to metallic Ni nanoparticles ($NiO + 2 Li^{2+} + 2 e^- \rightarrow Ni + Li_2O$) with concurrent formation of $Li_2O$ in the shell domain of hollow nanospheres and formation of solid electrolyte interface (SEI) layers.[45] On the first charge (anodic sweep), there is a broad anodic shelf that stretches from 1.3–1.68 V corresponding to partial decomposition of the polymeric coating on the NiO surface, while the decomposition of $Li_2O$ and oxidation of metallic nickel to NiO ($Ni + Li_2O \rightarrow NiO + 2 Li^+ + 2 e^-$) nanograins takes place at 2.33 V. These results are consistent with previous reports.[46,47] The second cathodic sweep differs from the first one; the strong peak at 0.27 V in the first scan vanished completely (broad peak) and a peak at 0.81 V is visible in the second scan corresponding to Li insertion and reduction of NiO to metallic lithium. However during second oxidation scanning, the oxidation peak positions were unaltered and oxidation of metallic Ni to NiO takes place at 2.34 V.

Fig. 6 exhibits discharge-charge curves in the voltage window of 0.005–3.0 V (vs. Li) at a rate of 0.3 C up to 50 cycles, and for clarity, only selected cycles are shown in the voltage versus capacity profiles. During the first cycle, the initial discharge and charge capacities are

1223 and 889 mAh.g$^{-1}$, respectively; the corresponding coulombic efficiency is 72.6 %. As it is

shown in the initial discharge curve, the voltage decreases sharply from 3.0 to 1.1 V and a

plateau region appears at about 0.75 V which is ascribed to formation of $Li_2O$, metallic Li, and

SEI layers consistent with the cyclic voltammogram results (Fig.5). The reaction mechanism of

NiO by Li was well demonstrated in the previous reports.[48,49] It involves the formation of highly

reactive nickel nanograins dispersed into $Li_2O$, which is the key to enable the formation-

decomposition of $Li_2O$ upon subsequent cycles, whereas Ni is converted back to NiO nanograins.

The plateau at 0.75 V extends up to the capacity of 860 mAh.g$^{-1}$ and then gradually reaches up

to 1223 mAh.g$^{-1}$ mainly due to electrolyte decomposition in the low-potential region and

subsequent formation of solid electrolyte interphase (SEI) on the NiO hollow particles. The

irreversible capacity loss observed in the first cycle is mainly due to irreversible loss of lithium

due to the formation of stable solid electrolyte interface (SEI) layer with the electrolytes and the

electrode and the formation of amorphous $Li_2O$.[45,50,51] Thus, the higher discharge capacity

observed in the first cycle could be attributed to the formation of the solid electrolyte interface

(SEI) layer. In addition, it is worth to note that the initial plateau and slope in the second and

subsequent cycles were less obvious than the first cycle, suggesting irreversible capacity loss in

the first cycle.

The discharge capacities of NiO electrode in the 1$^{st}$, 2$^{nd}$, 5$^{th}$, 25$^{th}$, and 50$^{th}$ cycles are

1223, 905, 872, 539, and 393 mAh.g$^{-1}$, respectively. The corresponding charge capacity values

are 889, 871, 829, 525, and 392 mAh.g$^{-1}$ for 1$^{st}$, 2$^{nd}$, 5$^{th}$, 25$^{th}$, and 50$^{th}$ cycles, respectively.

Furthermore, NiO-nanostrucutures like NiO thin-film on nickel metal foam and cobalt-doped

NiO nanoflakes as anode materials exhibited discharge capacities of 400 mAhg$^{-1}$ and 600

mAhg$^{-1}$, respectively, after 50 repeated cycles.[52,53] Thus these modified or composite NiO

nanoparticles show slightly higher discharge capacities due to improvement in electronic conductivity of nickel metal foam or doping compared with unmodified NiO hollow nanospheres. Nonetheless, the NiO hollow nanospheres exhibit very high capacity even after 50 cycles of charge-discharges (393 mAh.g$^{-1}$) compared to NiO nanotubes constructed electrode which exhibits less than 200 mAh.g$^{-1}$ after 20 cycles.[54] To further prove that, NiO nanotubes synthesized in the present study were also investigated as anode materials and showed similar discharge capacities which decreased to 221 mAhg$^{-1}$ from 1345 mAhg$^{-1}$ after 25 cycles of repeated charge/discharges (Supporting Information Fig. S7). In addition, in order to improve the capacity retention, we have also explored a composite containing NiO hollow particles and 7 Wt.% multi-walled carbon nanotubes (MWCNT) and 3 Wt.% SP carbon as electrode materials by replacing Teflonized acetylene black (TAB). Figure S8 shows the rate performance of the composite electrode comprised of NiO hollow nanospheres and MWCNT; the composite electrode clearly exhibits better capacity retention but are still prone to cycling stability during cycling processes as seen from cycling performance. However, the composite electrode shows higher discharge capacity after 50 cycles (458 mAhg$^{-1}$) than the NiO spherical hollow particles (393 mAh.g$^{-1}$). Fig.S9 shows the charge-discharge behavior of NiO dense micron sized particles; the discharge capacities in the 1$^{st}$, 2$^{nd}$, 5$^{th}$, 25$^{th}$, and 50$^{th}$ cycles are 464, 291,, 276, 209, and 182 mAh.g$^{-1}$, respectively. The corresponding charge capacities are 225, 221, 204, 168, and 167 mAh.g$^{-1}$ for 1$^{st}$, 2$^{nd}$, 5$^{th}$, 25$^{th}$, and 50$^{th}$ cycles respectively. Thus hollow nanospheres exhibit enhanced capacity than the nanotubes and/or micron sized dense NiO oxide due to the presence of hollow void space coupled with thin shell-walls in the former which facilitates fast Li transportation kinetics.

Fig.7 exhibits cycling performance of NiO hollow nanosphere constructed electrode up to

50 cycles of repeated charge-discharges at a rate of 0.3 C in the voltage window 0.005–3.0 V ($Li^+$ vs.Li). The charge-discharge capacities decrease gradually on increasing the rate or current density. Once initial cycle commences, the NiO nanoparticles is reduced to metallic nickel particles with even finer dimensions and this process further enhances electrochemical reactivity of transition metals (Ni in the present case). Thus the electrochemically produced metallic nickel nanograin enhances the electrolyte decomposition and lead to the extended formation of the SEI. During the formation of this film, charge transfer would be increasingly hindered and this phenomenon may explain the observed irreversible capacity losses and similar observation has also been made for NiO nanotubes.[50,54] The rate performance of NiO hollow nanospheres based electrode at different current densities is shown in Fig.8. The charge-discharge capacities decrease with increase of current densities similar to other nanostructured electrodes.[55] The NiO hollow nanosphere constructed electrode delivers discharge capacities of 1205, 1047, 889, 610, and 298 mAh.g$^{-1}$ during the first cycle as the rates (current densities) gradually vary from 0.1 C, 0.3 C, 1 C, 5 C, and 10 C, respectively. The NiO hollow particles constructed electrode exhibits highest discharge capacity of about 1205 mAh.g$^{-1}$ during the first cycle at 0.1 C rate and on further cycling, the discharge capacity is closer to 1100 mAh.g$^{-1}$ after 5 cycles. On increasing the rate to 0.3 C, 1 C, 5 C, and 10 C, the NiO electrode delivers a discharge capacity of 1205, 1047, 889, 610, and 298 mAh.g$^{-1}$ which is higher than the discharge capacity values reported for morphologically different NiO materials so far.[56-58] With gradually increasing the current rate, the capacity drops steadily similar to other material but the electrode regains its original capacity when the rate was again lowered to 0.3 C (1047 mAh.g$^{-1}$) indicative of better cycling stability of NiO hollow nanospheres based electrodes. To obtain microstructural stability of NiO hollow spherical particles, the particles were collected from coin-cell after 50 cycles and observed with

TEM for any morphological changes. It is seen from TEM image (supporting Information Fig. S10) that most of particles were retained their spherical morphology but deformation and rupturing of spherical particles have also been noticed to certain extent. These results prove high structural stability of NiO hollow nanosphere based electrodes. The enhanced charge capacity and rate capability of NiO hollow nanosphere can certainly be attributed to the hollow particles with a large void space with thin shell-matrix of about 10 nm. The thin-shell domain not only provides short Li-ion transport length due to small particle size but also favors Li transportation kinetics.[59] In addition, the void space effectively buffers against charge storage and the local volume changes during repeated charge/discharge process.[58] Furthermore, nanoparticle also provides good particle/electrolyte contact area, which account for the shorter Li diffusion pathway enhancing the rate performance.

**Conclusions**

We have successfully demonstrated a simple method for fabrication of NiO hollow nanospheres of size $28 \pm 2$ nm using polymeric micelles with *core-shell-corona* architecture as a soft template under optimum temperature. Low-temperature sol-gel reaction favored the formation of hollow particles with spherical morphology; whereas high-temperature synthesis conditions leads to formation nanotubes through morphological transformation of initial spherical micelles. The low-temperature synthesis invariably produced hollow nanospheres and TEM observation confirmed monodispersed hollow nanospheres with cavity size of $17 \pm 1$ and shell thickness of $11 \pm 1$ nm. X-ray diffraction pattern confirmed the formation of phase pure NiO with a cubic unit cell. The NiO hollow nanospheres constructed anode delivered high discharge capacity of 1223 mAh.g$^{-1}$ in the first cycle. The reversible capacity of NiO hollow nanospheres after 50 cycles

was found to be nearly two times higher than the NiO nanotubes. The improved electrochemical behavior is attributed to the nanosize effect coupled with hollow void space of NiO hollow particles that facilitates faster lithium ion insertion/deinsertion kinetics and also accounts for the volume changes taking place during the redox reactions.

**Acknowledgement**

## References

1       F. Caruso, R. A. Caruso and H. Möhwald, *Science* 1998, **282**, 1111.

2       Y. D. Yin, R. M. Rioux, C. K. Erdonmez, S. Hughes, G. A. Somorijai and A. P. Alivisatos, *Science* 2004, **304**, 711.

3       X. W. Lou, L. A. Archer and Z. Yang, *Adv. Mater.,* 2008, **20**, 3987.

4       A. N. Zelikin, O. Li and F. Caruso, *Angew. Chem. Int. Ed.,* 2006, **45**, 7743.

5       S. Ikeda, S. Ishino, T. Harada, N. Okamoto, T. Sakata, H. Mori, S. Kuwabata, T. Morimoto and M. Matsumura, *Angew. Chem. Int. Ed.,* 2006, **45**, 7063.

6       J. Yu, H. Guo, S. A. Davis and S. Mann, *Adv. Funct. Mater.,* 2006, **16**, 2035.

7       X. W. Lou, D. Deng, J. Y. Lee, J. Feng and L. A. Archer, *Adv. Mater*., 2008, **20**, 258.

8       R. K. Rana, V. S. Murthy, J. Yu and M. S. Wong, *Adv. Mater.,* 2005, **17**, 1145.

9       Q. R. Zhao, Y. Liu and H. Yan, *Chem. Commun.,* 2007, 2339.

10      Y. X. Hu, J. P. Ge, Y. G. Sun, T. R. Zhang and Y. D. Yin, *Nano Lett*., 2007, **7,** 1832.

11      Z. Yang, Z. Niu, Y. Lu, Z. Hu and C. C. Han, *Angew. Chem. Int. Ed.,* 2003, **42**, 1943.

12      M. Chen, L. M. Wu, S. X. Zhou and B. You, *Adv. Mater.,* 2006, **18**, 801.

13      P. M. Arnal, C. Weidenthaler and F. Schuth, *Chem. Mater.,* 2006, **18**, 2733.

14      X. W. Lou, C. Yuan and L. A. Archer, *Small* 2007, **3**, 261.

15      I. D. Hosein and C. M. Liddell, *Langmuir* 2007, **23**, 4832.

16      P. Jiang, J. F. Bertone and V. L. Colvin, *Science* 2001, **291**, 453.

17      Z. Zhong, Y. Yin, B. Gates and Y. Xia, *Adv. Mater.,* 2000, **12**, 206.

18      Y. Lu, Y. Yin and Y. N. Xia, *Adv. Mater.,* 2001, **13**, 271.

19    R. A. Caruso, A. Susha and F. Caruso, *Chem. Mater.,* 2001, **13**, 400.

20    D. E. Lynch, Y. Nawaz and T. Bostrom, *Langmuir,* 2005, **21**, 6572.

21    J. C. B. Kield, J. H. Jung and S. Shinkai, *Adv. Mater.,* 2001, **13**, 1472.

22    S. W. Kim, M. Kim, W. Y. Lee and T. Hyeon, *J. Am. Chem. Soc.,* 2002, **124**, 7642.

23    M. Sasidharan and K. Nakashima, *Acc. Chem. Res.* 2013, DOI. 10.1021/ar4001026.

24    A. Khanal, Y. Inoue, M. Yada and K. Nakashima, *J. Am. Chem. Soc.,* 2007, **129**, 1534.

25    M. Sasidharan, K. Nakashima, N. Gunawardhana, T. Yokoi, M. Inoue, S. Yusa, M. Yoshio and T. Tatsumi, *Chem. Commun.,* 2011, **47**, 6921.

26    M. Sasidharan, N. Gunawardhana, M. Inoue, S. Yusa, M. Yoshio and K. Nakashima, *Chem. Commun.,* 2012, **48**, 3200.

27    M. Sasidharan, N. Gunawardhana, H. Noma, M. Yoshio and K. Nakashima, *Bull. Chem. Soc. Jpn.,* 2012, **85**, 642.

28    M. Sasidharan, N. Gunawardhana, M. Yoshio and K. Nakashima, *J. Electrochem. Soc.,* 2012, **159**,  A618.

29    J. Park, E. Kang, S. U. Son, H. M. Park, M. K. Lee, J. Kim, K. W. Kim, H. J. Noh, J. H. Park, C. J. Bae, J. G. Park and T. Hyeon, *Adv. Mater.,* 2005, **17**, 429.

30    L. Li, E. A. Gibson, P. Qin, G. Boschloo, M. Gorlov, A. Hagfeldt and L. C. Sun, *Adv. Mater.,* 2010, **22**, 1759.

31    C. C. Yu, L. X. Zhang, J. L. Shi, J. J. Zhao, J. H. Gao and D. S. Yan, *Adv. Funct. Mater.,* 2008, **18**, 1544.

32    H. Pang, Q. Y. Lu, Y. C. Lia and F. Gao, *Chem. Commun.,* 2009, 7542.

33    S. Hosogai and H. Tsutumi, *J. Power Sources* 2009, **194**, 1213.

34    P. Poizot, S. Laruelle, S. Grugeon, L. Dupont and J. M. Tarascon, *Nature* 2000, **407**, 496.

35    M. N. Obrovac, R. A. Dunlap, R. J. Sanderson and J. R. Dahn, *J. Electrochem. Soc.,* 2001*,* **148**, A576.

36    S. Yusa, Y. Yokoyama and Y. Morishima, *Macromolecules* 2009*,* **42**, 376.

37    M. Sasidharan, D. Liu, N. Gunawardhana, M. Yoshio and K. Nakashima, *J. Mater. Chem*., 2011, **21**, 13881.

38    S. A. Needham, G. X. Wang and H. K. Liu, *J. Power Sources*, 2006, **159**, 254.

39    M. Sasidharan, H. N. Luitel, N. Gunawardhana, M. Inoue, S. Yusa, T. Watari and K. Nakashima, *Mater. Lett.,* 2012, **73**, 4.

40    M. Sasidharan, N. Gunawardhana, H.N. Luitel, T. Yokoi, M.  Inoue, S. Yusa, T. Watari, M. Yoshio, T. Tatsumi and K. Nakashima, *J. Colloid. Int. Sci.,* 2012, **370**, 51.

41    L. Liu, Y. Li, S. M. Yuan, M. Ge, M. M. Ren, C. S. Sun and Z. Zhou, *J. Phys. Chem. C* 2010, **114**, 251.

42    F. Chécot, S. Lecommandoux, Y. Gnagnou and H. A. Klok, *Angew. Chem. Int. Ed.* 2002, **41**, 1340.

43    S. Liu, J. V. M. Weaver, Y. Tang, N. C. Billingham, S. P. Armes and K. Tribe, *Macromolecules* 2002, **35**, 6121.

44    S. Minko, A. Kiriy, G. Gorodyska and M. Stamm, *J. Am. Chem. Soc.* 2002, **124**, 10193.

45    G. Gachot, S. Grugeon, M. Armand, S. Pilard, P. Guenot, J. M. Tarascon and S. Laruelle, *J. Power Sources* 2008, **178**, 409.

46    Y. J. Mai, J. P. Tu, X. H. Xia, C. D. Gu and X. L. Wang, *J. Power Sources* 2011, **196**, 6388.

47    Y. Wang, L. Qiao, X. Sun, X. Li, D. She, Q. Zhang and D. He, *J. Mater. Chem. A*, 2013, **1**,

4173.

48      P. Poizot, S. Laruelle, S. Grugeon, L. Dupont and J. M. Tarascon, *Nature* 2000, **407**, 496.

49      S. Grugenon, S. Laruelle, R. Herrera-Urbina, L. Dupont, P. Poizot and J. M. Tarascon, *J. Electrochem. Soc.* 2001, **148**, A285.

50      N. Munichandraiah, L. Scanlon and R. Marsh, *J. Power Sources* 1998, **72**, 203.

51      J. Li, S. Xiong, Y. Liu, Z. Ju and Y. Qian, *ACS Appl. Mater. Interfaces* 2013, **5**, 981.

52      Y.J. Mai, J. P. Tu, X. H. Xia, C. D. Gu and X. L. Wang, *J. Power Sources, 2011,* **196,** 6388.

53      J. Zhong, X.L. Wang, X. H. Xia, C. D. Gu, J. Y. Xiang, J. Zhang, J. P. Tu, *J. Alloys and Compounds*, 2011, **509**, 3889.

54      S. A. Needham, G. X. Wang and H. K. Liu, *J. Power Sources* 2006, **159**, 254.

55      P. G. Bruce, B. Scrosati and J. M. Tarascon, *Angew.Chem. Int. Ed.* 2008, **47**, 2930.

56      H. Liu, G. Wang, J. Lio, S. Qiao and H. Aha, *J. Mater. Chem.* 2011, **21**, 3046.

57      J. Ma, J. Yang, L. Jiao, Y. Mao, T. Wang, X. Duan, J. Lian and W. Zhang, *Cryst. Eng. Commun.* 2012, **14**, 452.

58      D. Liu, B. B. Garcia, Q. Zhang, Q. Guo, Y. Zhang, S. Sepehri and G. Cao, *Adv. Funct. Mater.* 2009, **19**, 1015.

59      H. Zhang, X. Yu and P. V. Braun, *Nat. Nanotechnol.* 2011, **6**, 277.
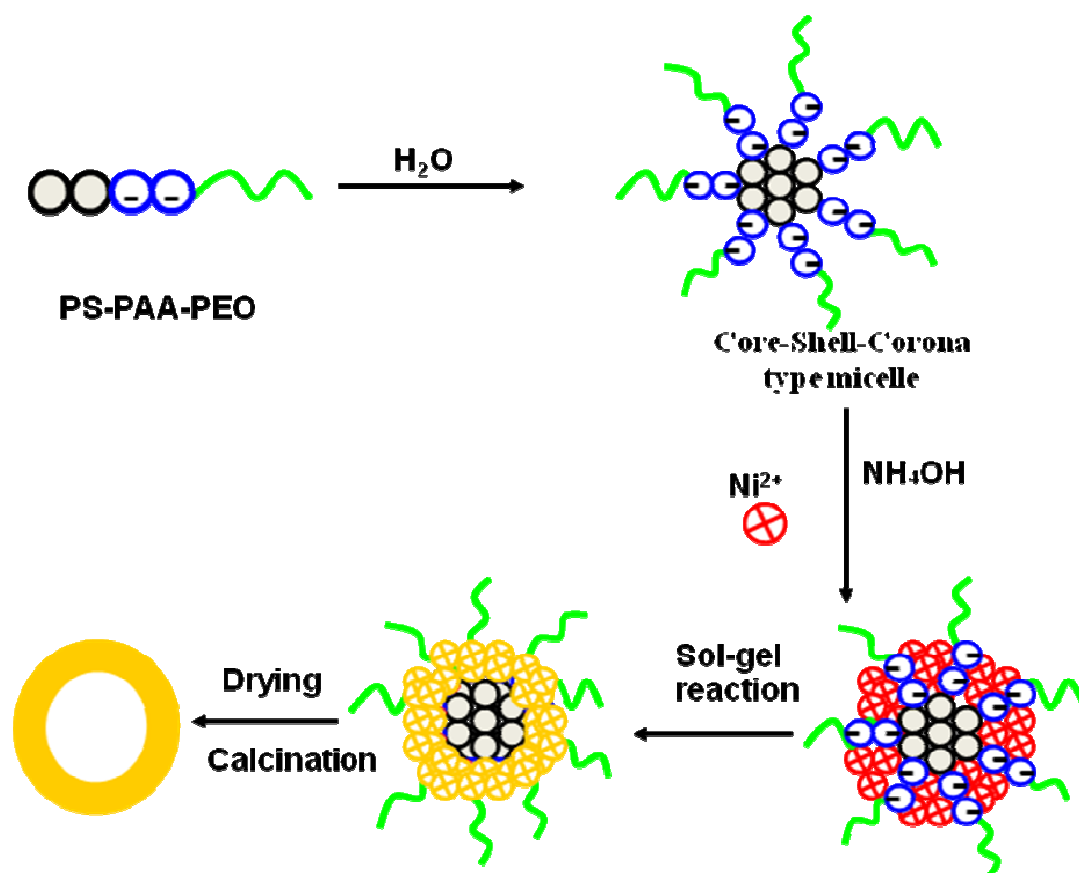
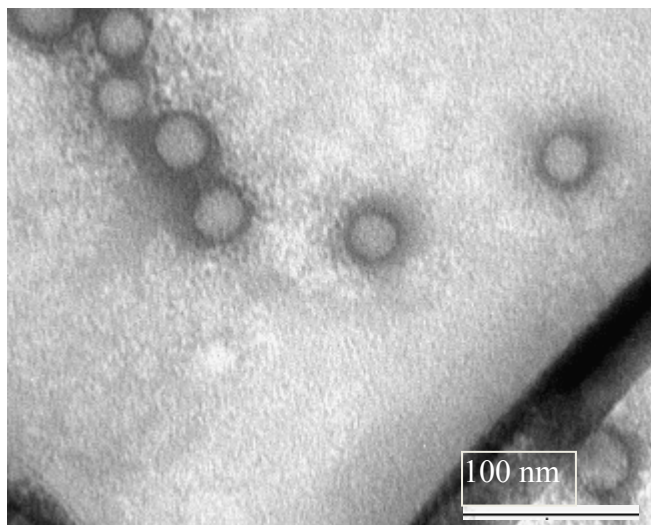**Scheme 1**. Schematic representation of formation of NiO hollow nanospheres.

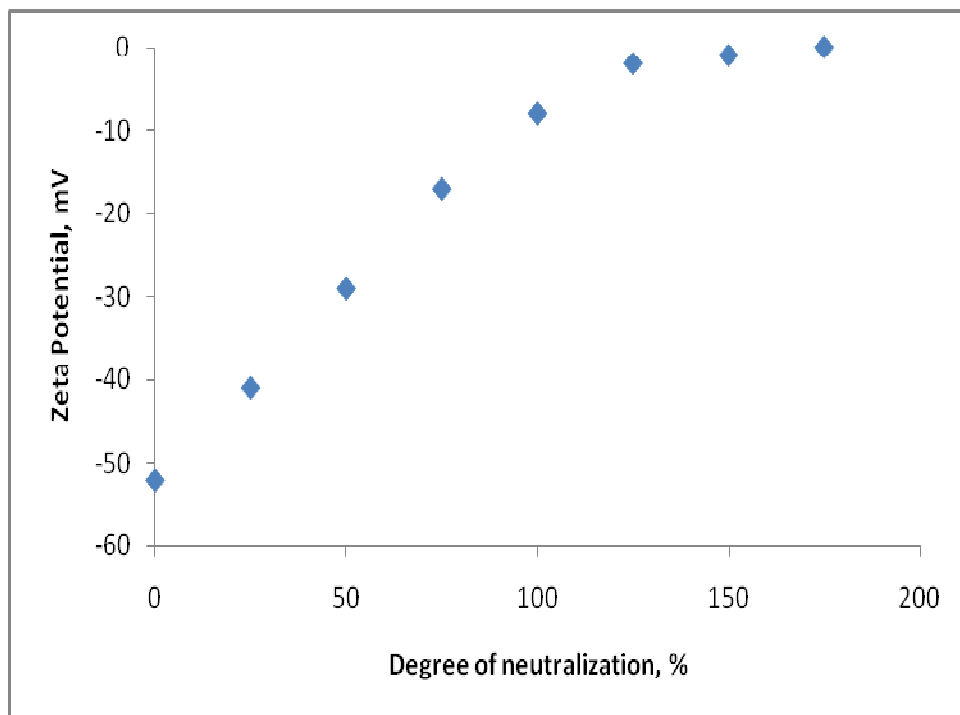**Fig.1** TEM image of the micelles of PS–PAA-PEO stained with phosphotungstic acid.

**Fig.2** Variation of zeta-potential due to charge neutralization of polyacrylic acid ($COO^-$)
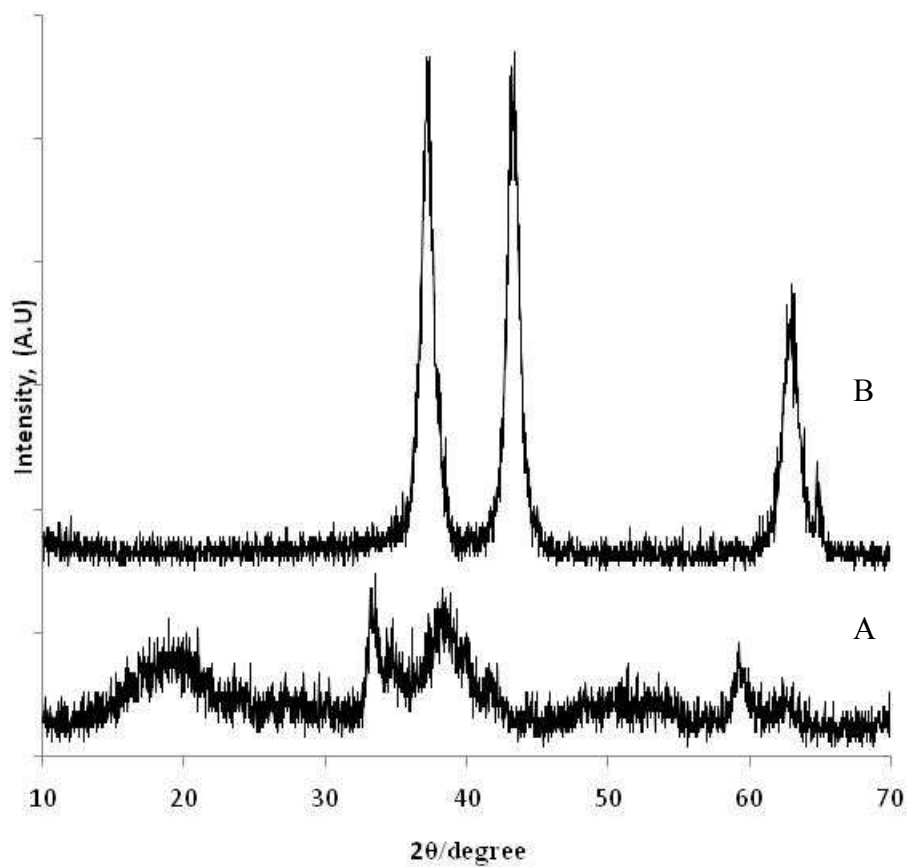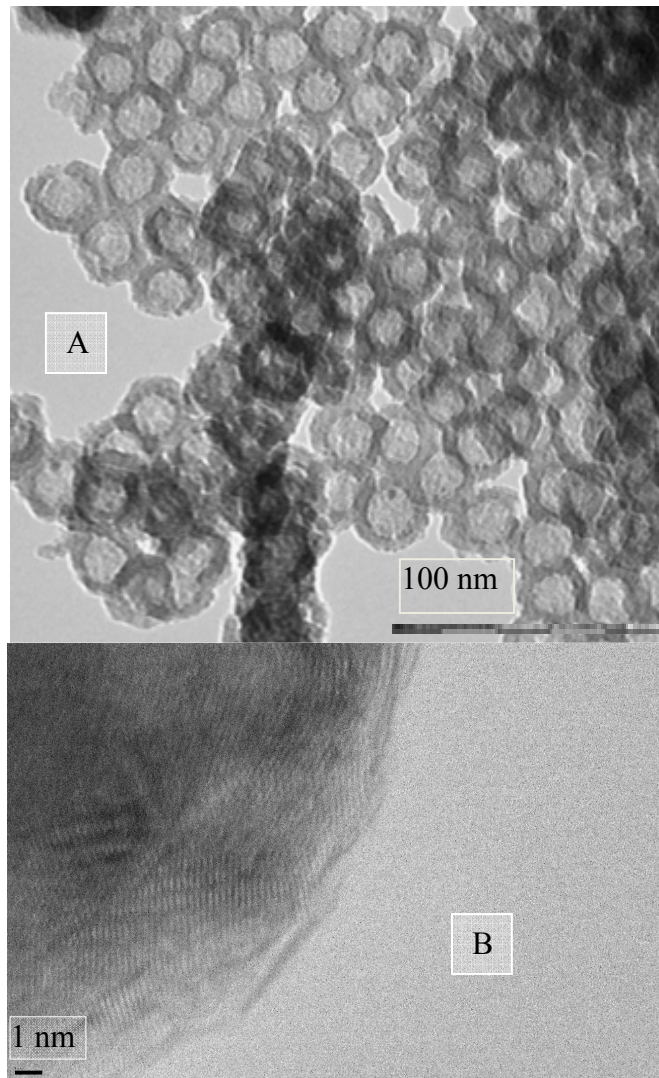
with $Ni^{2+}$ ions.

**Fig.3** Wide-angle XRD patterns of (A) polymer/$\alpha$-Ni(OH)$_2$ composite particles and (B) NiO hollow nanospheres.
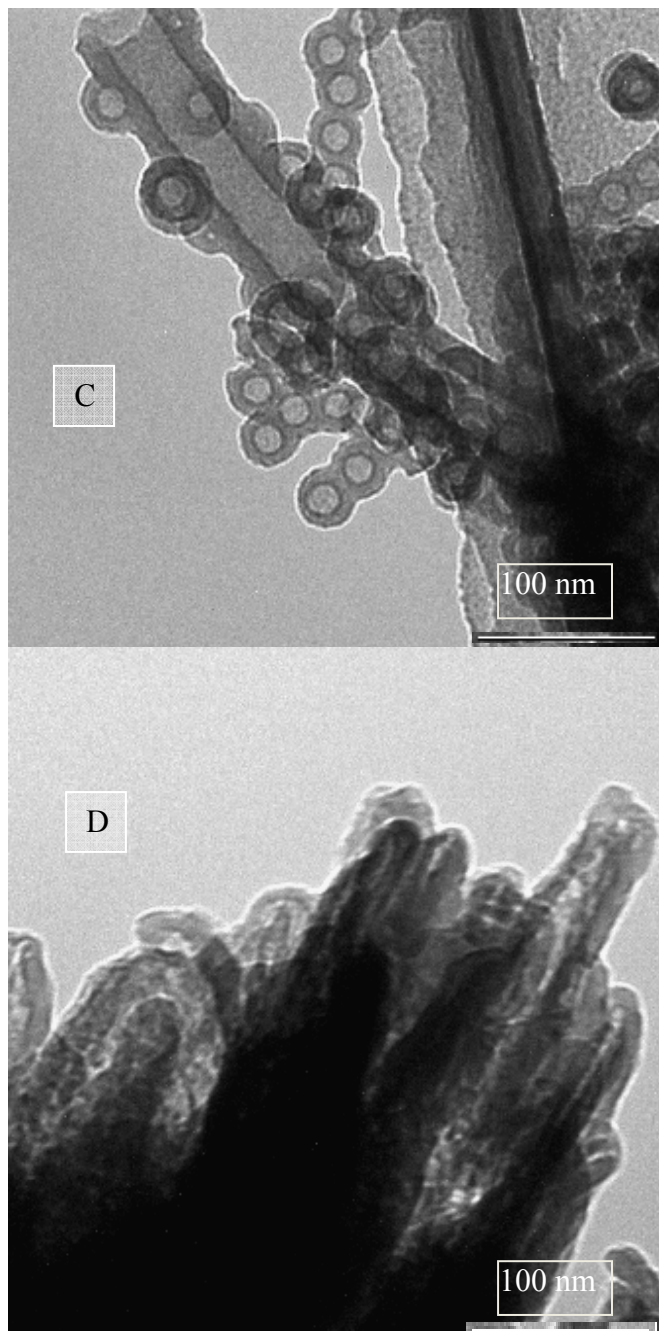
**Fig.4** TEM images of: (A) NiO hollow nanospheres; (B) HRTEM image of NiO hollow nanospheres; (C) Evolution of NiO nanotubes from hollow nanospheres, and (D) Aggregated nanotubes.
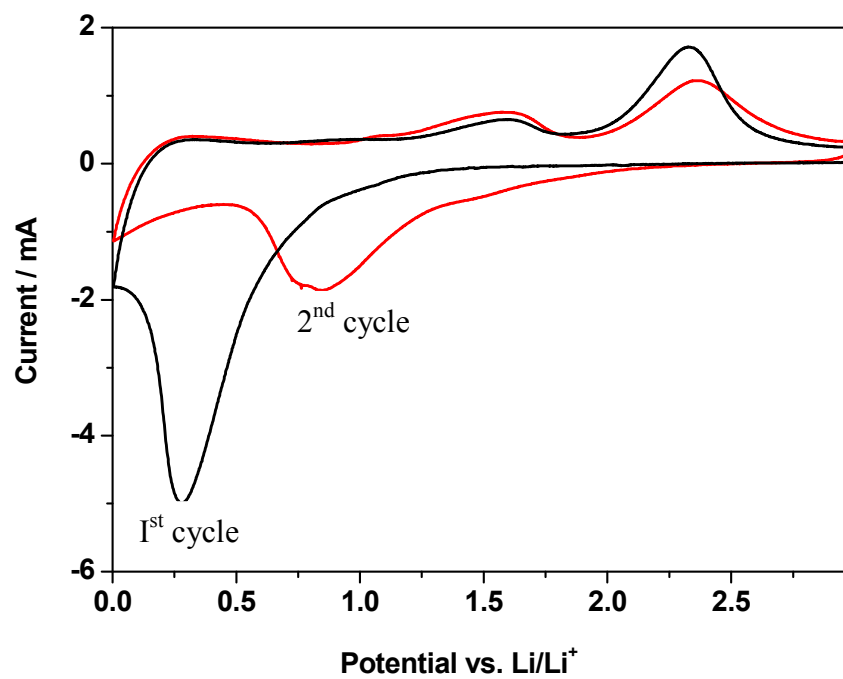
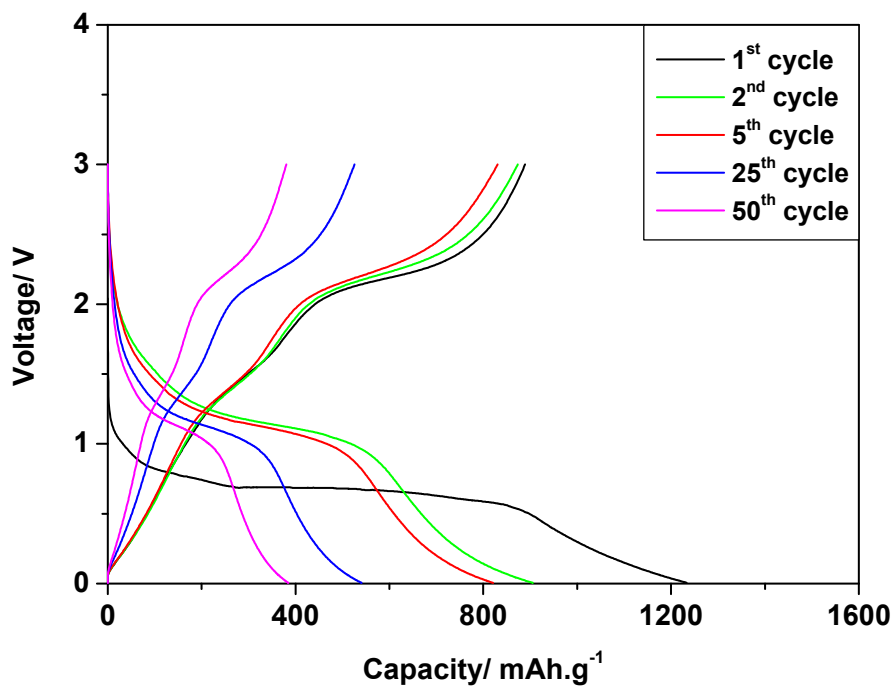**Fig.5** Cyclic voltammograms of NiO at a sweep rate of 3 mV/min. from 0.005–3.0 V (vs. Li$^+$/Li)

**Fig. 6** Galvanostatic charge/discharge curves of NiO electrodes between 0.005 V and 3.0 V (vs. Li/Li$^+$).
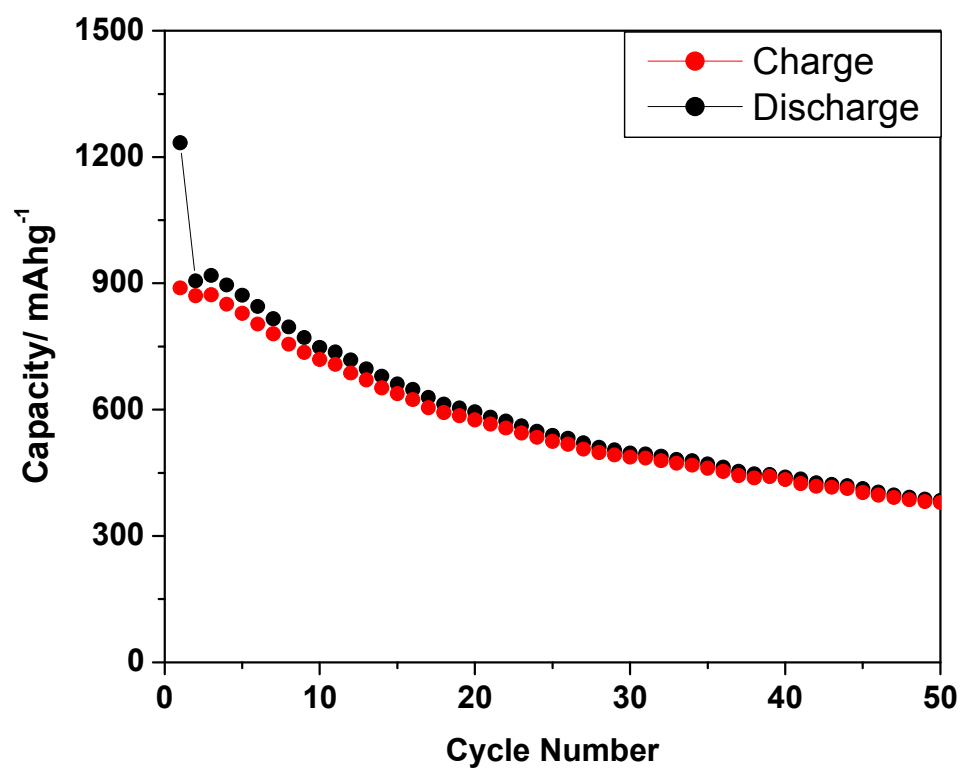
**Fig.7** Cycling performance of NiO hollow nanospheres for up to 50 cycles at a rate of 0.3 C in the voltage window of 0.005-3.0 V.
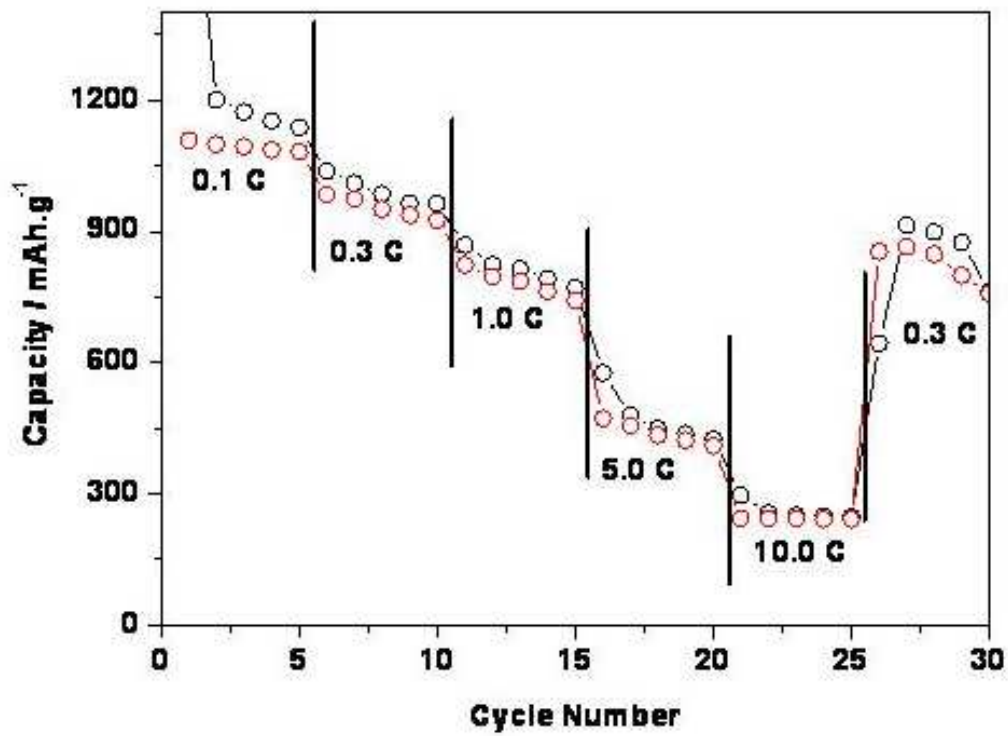
**Fig. 8** Rate performance of NiO hollow nanospheres at different current densities.